

## Energy transfer mechanism in a vibrating fluidized bed

Ting-Jie Wang<sup>a,b,\*</sup>, Yong Jin<sup>a</sup>, Atsushi Tsutsumi<sup>b</sup>, Zhanwen Wang<sup>a</sup>, Zhe Cui<sup>a</sup>

<sup>a</sup> Department of Chemical Engineering, Tsinghua University, Beijing 100084, China

<sup>b</sup> Department of Chemical System Engineering, The University of Tokyo, Tokyo 113-8656, Japan

Received 11 January 1999; received in revised form 20 March 2000; accepted 5 April 2000

### Abstract

The mechanism of vibration energy transfer in a vibrating fluidized bed (VFB) is reported in this paper. A series of sensors was employed to simultaneously detect pressure wave propagation signals at different positions at various heights in the fluidized bed. The mechanism of vibration energy transfer in an VFB is found by wave propagation. The pressure wave was produced from a vibrating base at the bed bottom and transferred to the particle bed via an air gap formed between the distributor and particle bed. The pressure waves oscillate and superpose in the fluidized bed due to wave reflection at the surface boundary and the bottom of the fluidized bed, leading to the wave energy dissipation being mainly in the bed. The wave propagation process and its mechanism in a fluidized bed have been analyzed. The pressure-wave propagation parameters were numerically calculated from the detected wave signals. The wave propagation velocities were found to be in the range of 9–75 m/s in the experiments. © 2000 Elsevier Science S.A. All rights reserved.

*Keywords:* Vibrating fluidized bed; Fluidization; Pressure wave; Wave propagation; Mechanism

### 1. Introduction

The vibrating fluidized bed (VFB) has been applied commercially to various processes, such as heat exchange, particle processing and chemical reaction, etc. The mechanical vibration imposed on a fluidized bed can significantly improve gas–solid contact and transport characteristics. It can be operated at a lower gas velocity and pressure drop compared to a conventional fluidized bed [1–4]. The empirical relationships of fluidization characteristics with operation parameters and particle properties in an VFB have been reported in many papers for various applications [5,6]. Recently, fluidization of fine particles has become more attractive in particle processing and chemical reaction. Due to a large particle–particle interaction, fine particles are difficult to fluidize [7–9]. Extra vibration energy is required to overcome the adhesion force between particles for the improvement of fluidization behavior. It is, therefore, essential to understand the energy transfer mechanism in the bed for proper operation or design of an VFB. The efficient transfer of mechanical energy in an VFB is essential in a practical application. Nevertheless, few papers have reported on the mechanism of vibration in the fluidized bed [1–3].

In a vibrated bed, a collision model of vibration energy transfer has been proposed while assuming an incompressible gas flow through a rigid particle bed [10]. Later, the collision model was improved by considering the gas to be compressible [11]. Based on that, the collision model was developed with new mathematical treatment to predict the collision state between the vibrating base and the particle bed at different vibration accelerations, and this model was found to be consistent with experimental results [12–14]. The mechanism of transmission of vibrating energy was considered to be such that the vibration body collides with the particles near the bottom and wall, and then these particles collide with the next particles, leading to the transmission of kinetic energy through the bed. Since considerable dissipation of particle kinetic energy occurs in any inelastic collision process, the penetration depth of the vibration energy into the bed is quite limited. Goldshtein et al. [15–18] observed a compression (shock) and expansion wave caused by vibration across the vibrated bed at a low frequency and large amplitude ( $f < 20$  Hz,  $A > 10$  mm) in a shallow bed. It was elucidated that the compression and expansion wave propagating across the bed balanced the loss of particle kinetic energy by inelastic collision. These waves govern the kinetic energy balance and sustain the collision hydrodynamic state of the vibrating bed.

Yamazaki et al. [1] observed that the large acceleration of mechanical vibration ( $>g$ ) causes pulsed gas flow through

\* Corresponding author. Tel.: +86-10-62785464; fax: +86-10-62772051.  
E-mail address: wangtj@mail.tsinghua.edu.cn (T.-J. Wang)

the bed at a low frequency (10–25 Hz) in an VFB, leading to pressure fluctuation in the VFB. The amplitude of the pressure fluctuation was affected by gas velocity, vibration frequency and vibration amplitude. Foscolo and Giblari [19,20] studied the transfer criteria of particulate and aggregate fluidization while considering the interaction force imparted on a particle by the surrounding fluid as a function of voidage. The motion of voidage fluctuation was taken as wave propagation in the fluidized bed. The wave propagation is affected by particles and fluid properties. The fluidization behavior can be evaluated from the wave growth rate.

Wang et al. [21] have reported that the energy transfer in a particle bed is mainly by collision before the bed is fluidized, but by wave propagation after the bed is fluidized. The shear forces of the vibration wave reduce the bubble size along the bed height.

In this study, the mechanism of vibration energy transfer in a VFB was studied. The propagation of a pressure wave was examined in an VFB by measuring the wave propagation signals along the fluidized bed.

## 2. Experimental

The experimental apparatus used in the present investigation is shown in Fig. 1. The VFB was made of a transparent acrylic resin cylinder with an 8-mm thickness, 200-mm inner diameter and 1000-mm height. A porous sintered stainless plate with holes of average diameter 25  $\mu\text{m}$  was used as a distributor in the fluidized bed. Porous and roughly spherical particles of goethite having an average diameter of 20  $\mu\text{m}$  and bulk density of 500  $\text{kg}/\text{m}^3$ , which were an agglomeration of needle-like particles with an average of 0.2- $\mu\text{m}$  length and 0.02- $\mu\text{m}$  radial diameter, were employed as one of the experimental powders. Their minimum fluidization velocity was 6 mm/s, from experiments. The other experimental powder was FCC particles with an average diameter of 54  $\mu\text{m}$  and bulk density of 1480  $\text{kg}/\text{m}^3$ . Their minimum fluidization velocity was 3 mm/s from experiments. The goethite and FCC particles are C and A class particles, respectively, according to Geldart's classification [22]. The static bed height ranged

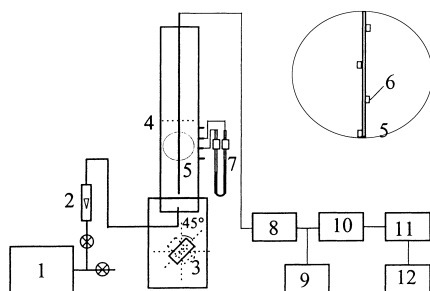


Fig. 1. The schematic diagram of the experimental apparatus. 1, air source; 2, flow meter; 3, vibration base; 4, fluidized bed; 5, sensor bar; 6, sensor; 7, micro-pressure meter; 8, amplifier; 9, oscilloscope; 10, signal filter; 11, A/D converter; 12, computer.

Table 1  
The sensitivities (in Pa/mV) of the different sensors in the experiments

Sensor no.								
1	2	3	4	5	6	7	8	9
9.069	9.706	9.938	9.524	10.246	8.884	7.913	6.010	7.971

from 280 to 400 mm. The static pressure along the bed height was measured from the side wall by micro-pressure meters placed at height intervals of every 40 mm. Fluidization gas velocity was varied in the range of 6–12 mm/s. Two vibration motors were cross mounted on opposite side walls of the vibrating base at an angle of 90° to produce a three-dimensional vibration. This was composed of a vertical vibration with a twist vibration in a tangential direction. Experiments showed a good gas–solid contact state with such a vibration style [23]. The vibration frequency range was 30–60 Hz, and amplitude 0.05–0.40 mm in experiments.

A condenser microphone of high sensitivity and good linear properties was employed to measure the pressure wave signals in the bed along the axial direction. This is a kind of capacitor-type sensor by which the pressure wave signals can be detected. The sensor had a cylindrical shape with a diameter of 6 mm. A stainless film of 0.06 mm thickness was pasted on the sensor terminal to make the microphone suit the powder environment in the bed. Nine sensors were fixed on a copper bar of 6 mm diameter to simultaneously measure the pressure wave signals along the bed height. The bar was centrally inserted in the bed and was made independent from the vibration body. The distance interval of adjacent sensors was 40 mm. The sensitivities of the film pasted sensors were checked with a standard microphone. The sensitivities of the sensors are shown in Table 1. The amplified electric signals from these sensors were monitored using an oscilloscope. The signals from the sensors were amplified and then sampled by computer. The sampling frequency  $f_s$  was set at 750 Hz. The sampling time of signals was 2.5 s. Any frequency higher than 200 Hz was filtered before sampling. The wave signals were analyzed by the FFT method.

## 3. Results and discussion

### 3.1. Wave propagation phenomena in the VFB

The pressure wave signals along the axial bed height in the VFB were detected by the nine sensors simultaneously. The pressure wave was observed to fill the whole bed, but no wave signals were detected outside the bed. The pressure wave signals at a nominal frequency of 30 Hz and their frequency spectra of power intensity and phase angle with FCC particles in the VFB are shown in Fig. 2. The fluidization gas velocity was 10 mm/s, which is higher than the minimum bubbling velocity of 4 mm/s. The dominant frequencies of the pressure wave were consistent with the frequencies of

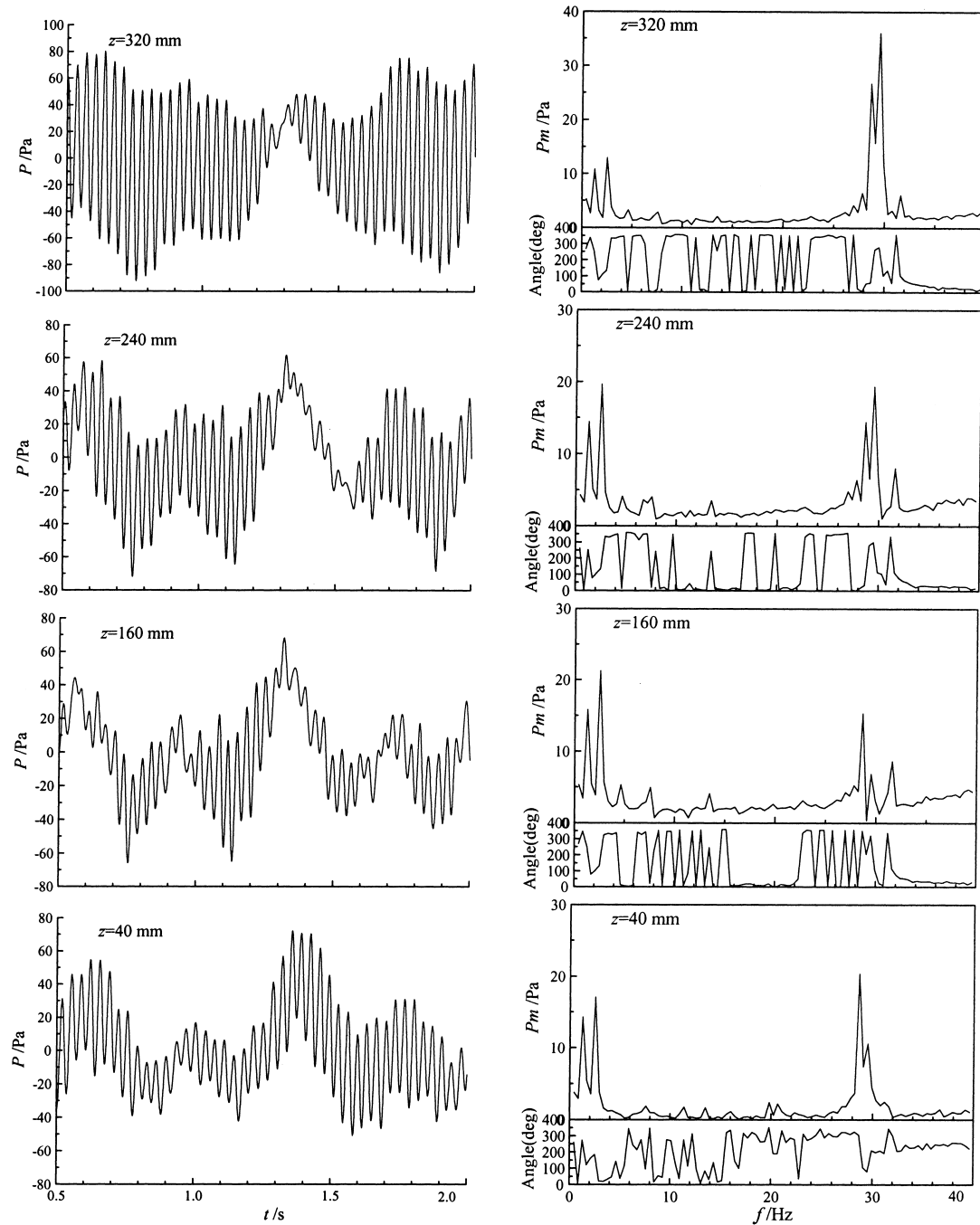


Fig. 2. The pressure wave signals and their frequency spectra in the VFB. FCC,  $H_0=400$  mm,  $H=425$  mm,  $u_g=10$  mm/s,  $f=30$  Hz,  $A=0.11$  mm.

the vibration body at about 28.7 and 29.5 Hz. Two frequencies result from the vibration motors running at slightly different speeds. The amplitude of the pressure wave at the top region ( $z=320$  mm) was found to be higher than that at the lower region. This is attributable to the reflection wave at the surface of the fluidized bed, which enhances the pressure wave signals. In the frequency spectra, two distinct peaks at 1–3 Hz were observed. These peaks can be assigned to bubble passing. The peaks at low frequencies become significant with increasing gas velocity [21].

In general, a complex wave can be expressed as a series of sinusoidal waves with different weights. Each of the sinusoidal waves propagates in a medium independently. The wave propagation characteristics can be studied by focusing on a single frequency sinusoidal wave. The single frequency wave propagating in an elastic medium causes a phase delay. In this study, the wave propagation process in the VFB was analyzed on the dominant single frequency fraction of 28.7 Hz. The phase change occurrence in the wave propagation process was observed in this experiment. The phase

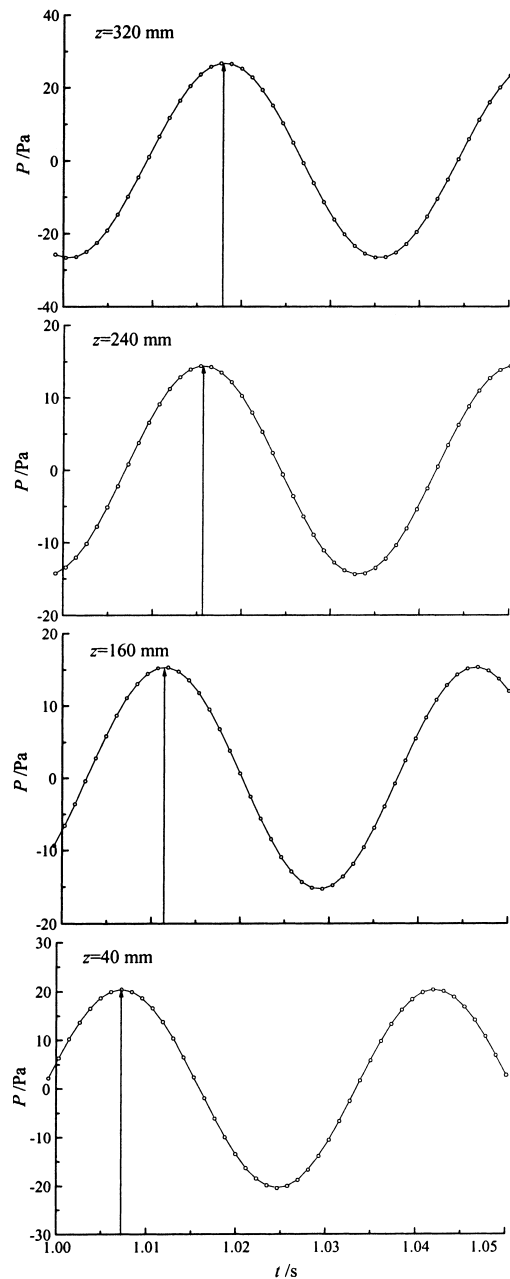


Fig. 3. The phase change of dominant pressure wave along the axial bed height. FCC,  $H_0=400$  mm,  $H=425$  mm,  $u_g=10$  mm/s,  $f=28.7$  Hz,  $A=0.11$  mm.

change at the dominant wave frequency of 28.7 Hz along the axial bed height in the VFB is shown in Fig. 3.

In a rigid body, the pressure fluctuation from the bottom is instantly transmitted through the rigid medium. No phase change occurs at any two points in the rigid medium, provided the vibration was transmitted throughout the medium. The phase change of the pressure wave in the fluidized bed shown in Fig. 3 indicates that the fluidized bed exhibits elasticity.

Experimental results showed that there is a distribution about the wave pressure amplitude along the bed height

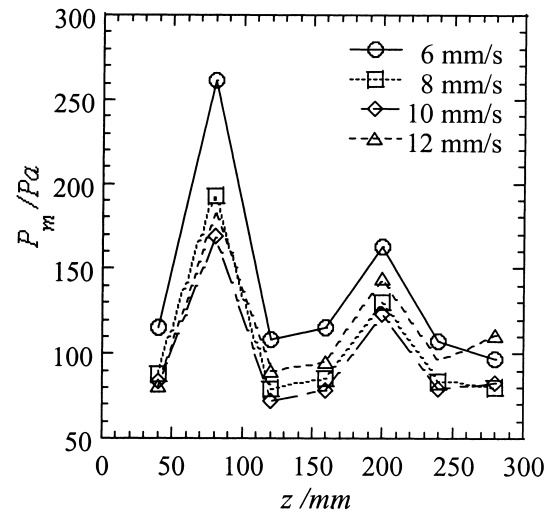


Fig. 4. The distribution of wave pressure amplitude at different fluidization gas velocities. Goethite,  $H_0=232$  mm,  $f=28.7$  Hz,  $A=0.36$  mm.

under certain conditions. The amplitude distribution basically demonstrates the energy distribution in the fluidized bed since the energy intensity is proportional to the square of the pressure wave amplitude in a uniform medium. This distribution was affected by the fluidization behavior in the bed. The pressure wave amplitude distribution at different fluidization gas velocities is shown in Fig. 4.

### 3.2. VFB medium for wave propagation

In the fluidized bed, each particle was surrounded by gas flow. Buoyancy and drag forces acting on particles caused by the gas flow enable the particles to move in the vertical direction with some elastic property [19]. Horizontal pressure caused by the vertical gas flow enables the particles to move with some elastic property in the horizontal direction. This mixture of continuous gas flow and discrete particles gives the bed the properties of an elastic medium. It is schematically shown in Fig. 5.

The particles suspended in the gas flow are mobile and affected by pressure fluctuation. When a pressure disturbance is introduced, the disturbance travels through the fluidized bed in the form of an elastic or pressure wave. In a

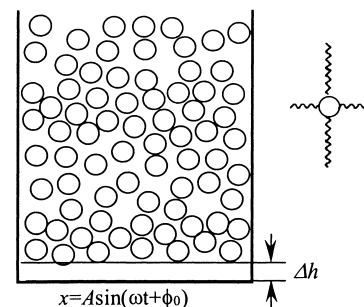


Fig. 5. The medium model of a fluidized bed for wave propagation.

bubbling fluidized bed, the medium of the bed is composed of a bubble phase and an emulsion phase. The boundary of the bubble phase and the emulsion phase results in a wave propagation parameter change in the VFB due to the different elastic properties in the two phases.

An air gap exists between the particle bed and the vibrating base in the VFB [13,14]. The particle bed is suspended in the gas flow. The base vibration produces a pressure fluctuation at the bottom of the bed, and the pressure fluctuation is transferred to the particle bed via the air gap instead of by direct collision between the vibration base and the particle bed. Thus, the energy transfer in the VFB is not by the collision of particles, but by the wave propagation through the elastic particle bed.

### 3.3. Wave propagation parameters in the VFB

In the case of mechanical wave propagation through an elastic medium, the wave propagation velocity depends on both the elastic and inertial properties of the medium. For a fluid medium, the wave propagation velocity,  $u$ , can be written as [24]

$$u = \sqrt{\frac{B}{\rho}} \quad (1)$$

where  $\rho$  is the fluid density and  $B$  the bulk modulus of the fluid medium. Considering the fluidized bed, the bulk modulus  $B$  of a fluidized bed medium can be expressed as

$$B = -\frac{P}{\Delta V/V} \quad (2)$$

where  $P$  is the wave pressure in the fluidized bed and  $\Delta V/V$  the volumetric strain under the stress  $P$ . The reciprocal of the bulk modulus  $B$  is the compressibility of the medium. The more rigid the medium is (i.e. the larger the  $B$ ), the faster is the wave propagation velocity in the medium.

Considering a certain volume  $V$  in the fluidized bed, the following expression can be given:

$$V = V_g + V_s \quad (3)$$

where  $V_g$  and  $V_s$  are the volumes of gas and solid phases, respectively. For the gas phase, the assumption of an ideal gas gives

$$P^*V_g = (P^* + P)(V_g + \Delta V_g) \quad (4)$$

where  $P^*$  is the absolute static pressure at a certain position in the fluidized bed, and  $\Delta V_g$  is the volume change of gas caused by wave pressure. Since the solid particles in the fluidized bed are incompressible, the combination of Eqs. (3) and (4) gives

$$\frac{\Delta V}{V} = \frac{\Delta V_g}{V} \equiv -\frac{\varepsilon P}{P^* + P} \quad (5)$$

where  $\varepsilon$  is the local voidage of the bed. Substituting Eq. (5) into Eq. (2), we obtain

$$B = \frac{P^* + P}{\varepsilon} \quad (6)$$

The local bulk density of the fluidized bed,  $\rho_b$ , can be written as

$$\rho_b = \frac{dP^*/dz}{g} \equiv \varepsilon\rho_g + (1 - \varepsilon)\rho_s \quad (7)$$

where  $\rho_g$  and  $\rho_s$  are the densities of gas and solid, respectively,  $g$  the acceleration due to gravity. Substituting Eqs. (6) and (7) into Eq. (1), yields

$$u(z) = \left\{ \frac{P^* + P}{\varepsilon[\varepsilon\rho_g + (1 - \varepsilon)\rho_s]} \right\}^{1/2} \quad (8)$$

In Eq. (8),  $P$  can be neglected compared to the absolute static pressure  $P^*$  in the fluidized bed, as the change of  $P^*$  along the bed height is quite limited since the value of atmosphere pressure ( $1.01325 \times 10^5$  Pa) is much larger than the pressure caused by the suspended particles in the bed. Therefore, the wave propagation velocity depends mainly on the local voidage. From Eq. (8), the wave propagation velocity in the fluidized bed can be estimated from the values of  $P^* + P$ ,  $\varepsilon$  and  $\rho_b$ . The wave propagation velocity estimated was in the range of 9–75 m/s in this experimental situation.

In the pressure wave propagation process, wave reflection occurs at the boundary of different media. The reflection coefficient of pressure amplitude is defined as [25]

$$R = \frac{Z_1 - Z_2}{Z_1 + Z_2} \quad (9)$$

$$Z = \sqrt{\rho_b B} \quad (10)$$

where  $R$  is the reflection coefficient of pressure wave amplitude, and  $Z_1$  and  $Z_2$  the specific acoustic impedances of incident medium and transmitted medium, respectively. In the fluidized bed, the wave reflection coefficients at the top surface boundary and bottom boundary approach a value of 1 as estimated from Eq. (9), because the bulk density of the fluidized bed is much higher than that of the air and the bulk modulus of the distributor at the bottom is much higher than that of the fluidized bed. Therefore, the pressure wave oscillates in the fluidized bed, causing the main dissipation of vibration wave energy to be within the bed. It was observed during the experiment that no wave signals were detected by sensors outside the bed. The detected signals within the fluidized bed were the superposition signals of many reflected waves.

Assuming that the pressure wave propagates in a uniform medium with an attenuation coefficient  $\alpha$ , the one-way pressure wave at the dominant frequency in the propagation process can be written as

$$P(z, t) = P_{m0} e^{-\alpha z} \sin \left[ \frac{2\pi}{\lambda} z - \omega t + \phi_0 \right] \quad (11)$$

Table 2

The pressure wave amplitude and phase angle at different positions in the fluidized bed

Parameters	z (mm)								
	40	80	120	160	200	240	280	320	360
<i>FCC</i> <sup>a</sup>									
$P_m$ (Pa)	20.40	94.40	12.29	15.34	20.48	14.42	42.72	26.72	51.44
$\phi$ (°)	307.44	279.52	342.64	351.03	10.64	34.11	52.05	59.07	67.80
<i>Goethite</i> <sup>b</sup>									
$P_m$ (Pa)	71.25	175.96	106.51	73.12	91.89	68.32	67.03		
$\phi$ (°)	189.33	192.20	194.34	197.38	202.19	204.52	207.04		

<sup>a</sup> FCC:  $H_0=400$  mm,  $H=425$  mm,  $u_g=10$  mm/s,  $f=28.7$  Hz,  $A=0.11$  mm.<sup>b</sup> Goethite:  $H_0=232$  mm,  $H=325$  mm,  $u_g=10$  mm/s,  $f=28.7$  Hz,  $A=0.36$  mm.

where  $P(z,t)$  is the wave pressure of the dominant frequency at time  $t$  and axial position  $z$ ,  $P_{m0}$  the initial pressure amplitude of the wave source,  $\omega$  and  $\lambda$  the angular frequency and wavelength of the pressure wave at the dominant frequency, respectively, and  $\phi_0$  the initial phase angle of the wave source, i.e. from the vibrating base.

The detected wave pressure at the dominant frequency can be expressed as

$$P(z, t) = \sum_{n=0}^{\infty} P_n(z) \sin[\phi_n(z) - \omega t] \quad (12)$$

where  $P_n(z)$  and  $\phi_n(z)$  are the pressure wave amplitude and

phase angle of the  $n$ th reflected wave. Eq. (12) can be recast as follows (after the derivation shown in the Appendix A):

$$P(z, t) = P_m(z) \sin \left[ \frac{2\pi}{\lambda} z - \omega t + \phi_0 + \delta(z) \right] \quad (13)$$

in Eq. (13),

$$P_m(z) = \frac{Y(z)}{C} P_{m0} e^{-\alpha z} \quad (14)$$

where

$$C = 1 + e^{-4\alpha H} + 2e^{-2\alpha H} \cos \left( \frac{4\pi H}{\lambda} \right) \quad (15)$$

$$Y(z) = \left\{ \left[ 1 + e^{-2\alpha H} \cos \frac{4\pi}{\lambda} H + e^{-2\alpha(H-z)} \cos \frac{4\pi}{\lambda} (H-z) + e^{-2\alpha(2H-z)} \cos \frac{4\pi}{\lambda} z \right]^2 + \left[ -e^{-2\alpha H} \sin \frac{4\pi}{\lambda} H + e^{-2\alpha(H-z)} \sin \frac{4\pi}{\lambda} (H-z) + e^{-2\alpha(2H-z)} \sin \frac{4\pi}{\lambda} z \right]^2 \right\}^{1/2} \quad (16)$$

$$\delta(z) = \arctan \left\{ \frac{-e^{-2\alpha H} \sin(4\pi/\lambda)H + e^{-2\alpha(H-z)} \sin(4\pi/\lambda)(H-z) - e^{-2\alpha(2H-z)} \sin(4\pi/\lambda)z}{1 + e^{-2\alpha H} \cos(4\pi/\lambda)H + e^{-2\alpha(H-z)} \cos(4\pi/\lambda)(H-z) + e^{-2\alpha(2H-z)} \cos(4\pi/\lambda)z} \right\} \quad (17)$$

Table 3

The wave propagation parameters calculated from the wave signals at different positions

Parameters	z (mm)							
	40–80	80–120	120–160	160–200	200–240	240–280	280–320	320–360
<i>FCC</i> <sup>a</sup>								
$\alpha$ (m <sup>-1</sup> )	0.1	0.2	0.8	1.6	3.8	0.3	0.1	0.8
$\Delta\delta$ (°)	-56.8	7.4	-19.9	-14.5	0.0	-0.9	-35.3	-16.9
$\lambda$ (m)	0.50	0.33	0.51	0.42	0.62	0.79	0.41	0.56
$u$ (m/s)	14.36	9.46	14.46	11.99	17.59	22.57	11.78	16.05
<i>Goethite</i> <sup>b</sup>								
$\alpha$ (m <sup>-1</sup> )	0.1	0.2	0.5	0.7	0.1	3.6		
$\Delta\delta$ (°)	-31.5	-20.9	-28.1	-8.39	-39.1	-3.05		
$\lambda$ (m)	0.41	0.63	0.46	1.10	0.38	2.57		
$u$ (m/s)	11.86	17.94	13.13	31.65	10.83	73.71		

<sup>a</sup> FCC:  $H_0=400$  mm,  $H=425$  mm,  $u_g=10$  mm/s,  $f=28.7$  Hz,  $A=0.11$  mm.<sup>b</sup> Goethite:  $H_0=232$  mm,  $H=325$  mm,  $u_g=10$  mm/s,  $f=28.7$  Hz,  $A=0.36$  mm.

In the above Eqs.,  $P_m(z)$  is the wave pressure amplitude,  $H$  the height of the fluidized bed, and  $Y(z)/C$  and  $\delta(z)$  the wave pressure amplitude and phase angle factors resulting from the superposition of the reflected waves at position  $z$ , compared with the wave propagation in an infinite medium. Therefore, the wave pressure amplitude distribution in the fluidized bed can be determined by Eqs. (13)–(16).

According to Eqs. (13) and (14), the wavelength and the attenuation coefficient can be calculated from wave amplitudes and phase angles at any two different positions using the following equations:

$$P_m(z_2)Y(z_1)P_{m0}e^{-\alpha z_1} - P_m(z_1)Y(z_2)P_{m0}e^{-\alpha z_2} = 0 \quad (18)$$

$$\Delta\phi = \Delta \left[ \frac{2\pi}{\lambda}z + \phi_0 + \delta(z) \right] \equiv \frac{2\pi}{\lambda}(z_2 - z_1) + \Delta\delta(z) \quad (19)$$

where  $\Delta\phi$  is the phase change between positions  $z_1$  and  $z_2$  from the FFT analysis on detected wave signals, and  $\Delta\delta(z)$  the phase change caused by the superposition of reflection waves, which is calculated from Eq. (17). By numerically solving Eqs. (18) and (19), the average attenuation coefficient and the wavelength in the fluidized bed can be calculated from the pressure amplitudes and phase angles of detected wave signals at two different position,  $z_1$  and  $z_2$ . The pressure wave amplitude and phase angles from the FFT analysis on the detected wave signals in the fluidized bed at different positions with FCC and goethite particles are shown in Table 2. The average wavelengths and wave propagation velocities calculated from experimental wave signals at every two adjacent positions are shown in Table 3. The average wavelength in the fluidized bed is in the range of 0.3 to 2.6 m, and the wave propagation velocity is in the range of 9 to 75 m/s in these experiments. The wave velocity and wavelength in the fluidized bed are determined by the fluidization behavior.

It can be seen in Table 3 that the local properties of the fluidized bed affect the wave propagation parameters. The phase change detected simultaneously from the sensors along the axial height of the bed is different from the phase delay in the propagation process due to the  $\Delta\delta(z)$  item caused by the superposition of reflected waves.

#### 4. Conclusion

The mechanism of vibration energy transfer in a VFB was investigated in this research. The energy transfer from the vibrating base to the particle bed and the energy transfer in the VFB are by pressure wave propagation. The wave energy is mainly dissipated in the fluidized bed by the wave oscillation caused by wave reflection at the medium boundary at both top and bottom. The wave propagation process and its mechanism in a fluidized bed were analyzed. The wave propagation parameters are affected by fluidization behavior. A distribution of pressure wave amplitude in the fluidized bed exists in the experimental conditions. The wave propagation

velocities in the fluidized bed can be estimated by numerical analysis of experimental pressure wave signals, and are in the range of 9 to 75 m/s.

#### 5. Nomenclature

$A$	vibration amplitude (mm)
$B$	bulk modulus ( $\text{N m}^{-2}$ )
$C$	letter used to represent a function for simplifying an equation (dimensionless)
$f$	vibration frequency (Hz)
$f_s$	sampling frequency (Hz)
$g$	acceleration due to gravity ( $\text{m s}^{-2}$ )
$\Delta h$	air gap thickness (mm)
$H$	bed height (mm)
$H_0$	static bed height (mm)
$P$	wave pressure ( $\text{N m}^{-2}$ )
$P_m$	pressure wave amplitude ( $\text{N m}^{-2}$ )
$P_n$	pressure wave amplitude of the $n$ th reflected wave ( $\text{N m}^{-2}$ )
$P^*$	absolute static pressure in the fluidized bed ( $\text{N m}^{-2}$ )
$R$	reflection coefficient of pressure wave amplitude (dimensionless)
$t$	time (s)
$u$	wave velocity ( $\text{m s}^{-1}$ )
$u_g$	fluidization gas velocity ( $\text{mm s}^{-1}$ )
$V$	volume ( $\text{m}^3$ )
$V_g$	volume of gas phase in fluidized bed ( $\text{m}^3$ )
$V_s$	volume of solid phase in fluidized bed ( $\text{m}^3$ )
$\Delta V$	volume change under wave pressure ( $\text{m}^3$ )
$x$	displacement of vibration base (mm)
$Y$	letter used to represent a function for simplifying an equation (dimensionless)
$z$	axial height in the bed (mm)
$z_1$	axial height in the bed at $z_1$ position (mm)
$z_2$	axial height in the bed at $z_2$ position (mm)
$Z$	specific acoustic impedance ( $\text{kg m}^{-2} \text{s}^{-1}$ )
$Z_1$	specific acoustic impedance of incident medium ( $\text{kg m}^{-2} \text{s}^{-1}$ )
$Z_2$	specific acoustic impedance of transmitted medium ( $\text{kg m}^{-2} \text{s}^{-1}$ )

#### Greek symbols

$\alpha$	attenuation coefficient of pressure wave amplitude ( $\text{m}^{-1}$ )
$\delta$	phase angle caused by superposition of wave reflection ( $^\circ$ )
$\Delta\delta$	phase change caused by reflected waves at different positions ( $^\circ$ )
$\varepsilon$	local voidage in fluidized bed (dimensionless)
$\phi$	phase angle ( $^\circ$ )
$\phi_n$	phase angle of the $n$ th reflected wave ( $^\circ$ )
$\lambda$	wavelength (m)

$\rho$	density ( $\text{kg m}^{-3}$ )
$\rho_b$	bulk density of the fluidized bed ( $\text{kg m}^{-3}$ )
$\rho_g$	density of fluidization gas ( $\text{kg m}^{-3}$ )
$\rho_s$	densities of particles ( $\text{kg m}^{-3}$ )
$\omega$	angle frequency ( $\text{s}^{-1}$ )

## Acknowledgements

The authors wish to express their appreciation for the financial support of this study by the National Natural Science Foundation of China. The grant number is 29776029.

## Appendix A

The wave reflection at the top and bottom boundary is schematically shown in Fig. 6. To simplify the derivation process, consider the function

$$\begin{aligned} \frac{P^+(z, t)}{P_{m0}} &= e^{-\alpha z + i((2\pi/\lambda)z - \omega t + \phi_0)} \\ &\equiv e^{-\alpha z} \cos \left[ \frac{2\pi}{\lambda} z - \omega t + \phi_0 \right] \\ &\quad + i e^{-\alpha z} \sin \left[ \frac{2\pi}{\lambda} z - \omega t + \phi_0 \right] \end{aligned} \quad (\text{A.20})$$

Taking into account the fact that the incident wave reflecting at the bottom boundary loses a half wavelength in phase angle because the specific acoustic impedance of the distributor is much higher than that of the fluidized bed [25], the superposed wave can be written as

$$\begin{aligned} \frac{P^+(z, t)}{P_{m0}} &= e^{-\alpha z + i((2\pi/\lambda)z - \omega t + \phi_0)} \\ &\quad + e^{-\alpha(2H-z) + i((2\pi/\lambda)(2H-z) - \omega t + \phi_0)} \\ &\quad + e^{-\alpha(2H+z) + i((2\pi/\lambda)(2H+z + \lambda/2) - \omega t + \phi_0)} \\ &\quad + e^{-\alpha(4H-z) + i((2\pi/\lambda)(4H-z + \lambda/2) - \omega t + \phi_0)} \\ &\quad + \dots + e^{-\alpha(2nH+z) + i((2\pi/\lambda)(2nH+z + n\lambda/2) - \omega t + \phi_0)} \\ &\quad + e^{-\alpha[2(n+1)H-z] + i((2\pi/\lambda)[2(n+1)H-z + n\lambda/2] - \omega t + \phi_0)} \\ &\quad + \dots = e^{-\alpha z + i((2\pi/\lambda)z - \omega t + \phi_0)} \\ &\quad \times [1 + e^{-2\alpha(H-z) + i(4\pi/\lambda)(H-z)}] \\ &\quad \times \sum_{n=0}^{\infty} (-1)^n (e^{-2\alpha H + i(4\pi/\lambda)H})^n \end{aligned} \quad (\text{A.21})$$

Since  $\sum_{n=0}^{\infty} (-1)^n x^n = 1/(1+x)$ , we can reduce Eq. (A.21) thus:

$$\begin{aligned} \frac{P^+(z, t)}{P_{m0}} &= \frac{e^{(-\alpha z + i((2\pi/\lambda)z - \omega t + \phi_0))} [1 + e^{(-2\alpha(H-z) + i(4\pi/\lambda)(H-z))}]}{1 + e^{(-2\alpha H + i(4\pi/\lambda)H)}} \end{aligned} \quad (\text{A.22})$$

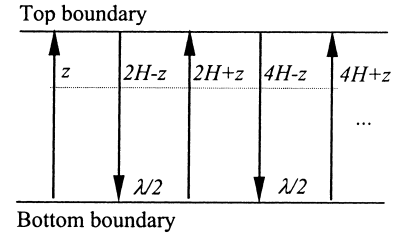


Fig. 6. Schematic diagram of wave reflection at the top and bottom boundary.

By multiplying the numerator and denominator in the right-hand side of Eq. (A.22) by  $1 + e^{(-2\alpha H - i(4\pi/\lambda)H)}$ , we obtain

$$\begin{aligned} \frac{P^+(z, t)}{P_{m0}} &= \frac{e^{(-\alpha z + i((2\pi/\lambda)z - \omega t + \phi_0))} [1 + e^{(-2\alpha(H-z) + i(4\pi/\lambda)(H-z))} + e^{(-2\alpha H - i(4\pi/\lambda)H)} + e^{(-2\alpha(2H-z) - i(4\pi/\lambda)z)}]}{1 + e^{(-4\alpha H)} + \cos(4\pi H/\lambda)} \end{aligned} \quad (\text{A.23})$$

After evolving Eq. (A.23), the imaginary part was taken as the pressure wave signal, yielding

$$P(z, t) = \frac{Y(z)}{C} P_{m0} e^{-\alpha z} \sin \left[ \frac{2\pi}{\lambda} z - \omega t + \phi_0 + \delta(z) \right] \quad (\text{A.24})$$

where

$$C = 1 + e^{-4\alpha H} + 2e^{-2\alpha H} \cos \left( \frac{4\pi H}{\lambda} \right) \quad (\text{A.25})$$

$$\begin{aligned} Y(z) &= \left\{ \left[ 1 + e^{-2\alpha H} \cos \frac{4\pi}{\lambda} H + e^{-2\alpha(H-z)} \cos \frac{4\pi}{\lambda} (H-z) \right. \right. \\ &\quad \left. \left. + e^{-2\alpha(2H-z)} \times \cos \frac{4\pi}{\lambda} z \right]^2 + \left[ -e^{-2\alpha H} \sin \frac{4\pi}{\lambda} H \right. \right. \\ &\quad \left. \left. + e^{-2\alpha(H-z)} \sin \frac{4\pi}{\lambda} (H-z) \right. \right. \\ &\quad \left. \left. + e^{-2\alpha(2H-z)} \sin \frac{4\pi}{\lambda} z \right]^2 \right\}^{1/2} \end{aligned} \quad (\text{A.26})$$

$\delta(z) = \arctan$

$$\times \left\{ \frac{-e^{(-2\alpha H)} \sin(4\pi/\lambda)H + e^{(-2\alpha(H-z))} \sin(4\pi/\lambda) \times (H-z) - e^{(-2\alpha(2H-z))} \sin(4\pi/\lambda)z}{1 + e^{(-2\alpha H)} \cos(4\pi/\lambda)H + e^{(-2\alpha(H-z))} \cos(4\pi/\lambda) \times (H-z) + e^{(-2\alpha(2H-z))} \cos(4\pi/\lambda)z} \right\} \quad (\text{A.27})$$

## References

- [1] R. Yamazaki, Y. Kanagawa, G. Jinbo, Heat transfer in vibro-fluidized bed: effect of pulsated gas flow, J. Chem. Eng. Jpn. 7 (1974) 373–378.

- [2] R. Gupta, A.S. Mujumdar, Aerodynamics of a vibrated fluid bed, *Can. J. Chem. Eng.* 58 (1980) 332–338.
- [3] R. Gupta, A.S. Mujumdar, Aerodynamic and thermal characteristics of vibrated fluid beds — review, in: A.S. Mujumdar, *Drying'80*, Vol. 1, Hemisphere, New York, 1980, pp. 141–149.
- [4] J.M. Beeckmans, K. Macwilliam, Stabilization of a fluidized bed by horizontal vibrations, *Powder Technol.* 45 (1986) 177–181.
- [5] E.A. Bratu, G.I. Jinescu, Heat transfer in vibrated fluidized layers, *Rev. Roum. Chim.* 17 (1) (1972) 49–56.
- [6] V.I. Mushtaev, V.A. Chevilenko, B.M. Korotkov, Investigation of drying of granular materials in apparatus with a vibro-fluidized bed, *Teoret. Osn. Khim. Tekhnol.* 8 (6) (1974) 220–225.
- [7] J. Chaouki, C. Chavarie, D. Klavana, G. Pajonk, Effect of interparticle forces on the hydrodynamic behavior of fluidized aerogels, *Powder Technol.* 43 (1985) 117–125.
- [8] J. Visser, An invited review — van der Waals and other cohesive forces affecting powder fluidization, *Powder Technol.* 58 (1989) 1–10.
- [9] S. Morooka, T. Okubo, K. Kusakabe, Recent work on fluidized processing of fine particles as advanced materials, *Powder Technol.* 63 (1990) 105–112.
- [10] W. Kroll, Über das verhalten von schuttgut in lotrecht schwingenden gefaßen, *Forshung.* 20 (1954) 2–15.
- [11] R. Gutman, Vibrated bed of powders. Part 1. A theoretical model for the vibrated bed, *Trans. Inst. Chem. Eng.* 54 (1976) 174–183.
- [12] T. Akiyama, T. Naito, Vibrated beds of powders: a new mathematical formulation, *Chem. Eng. Sci.* 42 (1987) 1305–1311.
- [13] T. Akiyama, H. Kurimoto, Compressible gas model of vibrated particle beds, *Chem. Eng. Sci.* 43 (1988) 2645–2653.
- [14] T. Akiyama, H. Kurimoto, The impulse of the collision between vibrating particle beds and a vessel base, *Chem. Eng. Sci.* 44 (1989) 427–431.
- [15] A. Goldshtein, M. Shapiro, L. Moldavsky, M. Fichman, Mechanics of collisional motion of granular materials. Part 2. Wave propagation through vibrofluidized granular layers, *J. Fluid Mech.* 287 (1995) 349–382.
- [16] A. Goldshtein, M. Shapiro, C. Gutfinger, Mechanics of collisional motion of granular materials. Part 3. Self-similar shock-wave motion, *J. Fluid Mech.* 316 (1996) 29–51.
- [17] A. Goldshtein, M. Shapiro, C. Gutfinger, Mechanics of collisional motion of granular materials. Part 4. Expansion wave, *J. Fluid Mech.* 327 (1996) 117–138.
- [18] A. Goldshtein, M. Shapiro, Vibrofluidized beds of solid granules: from experiments to hydrodynamic model, in: *Proceedings of Conference on Powders and Grains 97*, Rotterdam, 1997, pp. 381–384.
- [19] P.U. Foscolo, L.G. Giblari, A fully predictive criterion for the transition between particulate and aggregate fluidization, *Chem. Eng. Sci.* 39 (1984) 1667–1675.
- [20] P.U. Foscolo, L.G. Giblari, Fluid dynamic stability of fluidised suspensions: the particle bed model, *Chem. Eng. Sci.* 42 (1987) 1489–1500.
- [21] T.J. Wang, Y. Jin, Z. Wang, Z. Yu, Characteristics of wave propagation in a vibrating fluidized bed, *Chem. Eng. Technol.* V20N9 (1997) 606–611.
- [22] D. Geldart, Types of gas fluidization, *Powder Technol.* 7 (1973) 285–292.
- [23] S. Mori, A. Yamamoto, S. Iwata, T. Haruta, I. Yamada, E. Mizutani, Vibro-fluidization of group-C particles and its industrial applications, *AIChE Symp. Series* 86 (276) (1990) 88–94.
- [24] R.A. Serway, *Physics for Scientists and Engineers with Modern Physics*, 3rd Edition, Saunders College Publishing, London, 1990, pp. 456–460.
- [25] Y. Nagaoka, *Vibration and Wave*, Shoka-bo Publishing House, 1992.